CHAPTER 3

THERMODYNAMIC MODELING OF SOFC–GT–ST CYCLE

3.1 Introduction

The history of combined-cycle (CC) power plants dates back to 1949 when the first CC plant was installed in the US using the exhaust gas energy of a 3.5 MW GT unit to heat feed water for a 35 conventional ST plant [1]. CC plants using a GT (Brayton) and a ST (Rankine) cycle respectively as topping and bottoming cycle, offer higher thermal efficiency than either of the cycles executed individually. Therefore, CC power plants have found widespread commercial application and are receiving major attention throughout the world as one of the most effective energy conversion technologies [2]. The CC technology today is well developed and has been widely accepted in the fossil-fired power plants due to its higher efficiency [3]. GT in combination with heat recovery steam generator (HRSG) and ST represents the state of the art technology of the CC with efficiencies up to 60% in various plant capacities ranging from medium to large scale power generation [4, 5]. The HRSG is the most crucial component in a CC plant, which utilizes the waste energy of the GT exhaust gases for generating steam for the bottoming ST cycle. CC plants are more suitable in countries where natural gas is sufficiently available for electricity generation. All major GT manufacturing companies (GE, ABB, Westinghouse-Siemensetc.) are therefore nowadays actively engaged in manufacturing of new CC plants in various power ranges and replacing existing individual GT based or ST based power units [5]. In a recent article in March 2017, Rice [6] has reported about achieving a record 62.22 % efficiency by one of the GE manufactured natural gas burnt 605 MW CC power plants. But the quest for higher efficiency continue and as a result, innovative power cycles are still being developed and proposed by the power plant community in order to increase the level of efficiency even higher, particularly in small scale application where it shows usually low performance. Attention of the whole power community is focused on efficiency improvement and emission reduction due to ever increasing demand for energy and concern for the environment and depleting fossil fuel resources. Hybrid cycles involving a high temperature SOFC and bottoming heat engine cycles are some of such innovative, efficient and low emitting cycles that have been viewed as potential technology for future power generation. These hybrid SOFC power

technologies might help in meeting the future energy demands with enhanced efficiency, fuel flexibility, reliability, and reduced environmental impact. SOFC integrated hybrid CC plants exhibit synergies not present in typical combined cycles with efficiencies higher than either the SOFC or the CC plant alone.

In this chapter, a novel SOFC integrated CC plant is proposed, discussed and analyzed. The detailed thermodynamic model developed for each individual component of the topping SOFC–GT cycle and bottoming ST cycle is described with their theoretical background. The proposed new SOFC–GT–ST configuration has the provision for fuel and air preheating utilizing GT exhaust gas, additional fuel burning and steam extraction from the ST for fuel reforming in the PR. The plant utilizes the GT exhaust heat for fuel and air preheating subsequently in a FR and an AR before finally producing steam in a heat recovery steam generator (HRSG) coupled with the ST cycle. The steam required for fuel reforming in the PR is extracted from the ST at the desired pressure.

3.2 Description of system layout

The system layout of the SOFC integrated combined cycle is schematically shown in Fig. 3.1. All the system components are numerically modeled to evaluate the steady state performance of the proposed plant configuration. Energy and exergy balance is applied to each system component for determining the inlet and outlet conditions of the flow stream and the component irreversibility. Methane fuel is used which is first compressed in the fuel compressor (FC) and a certain fixed amount of compressed fuel is channeled to the SOFC anode via the fuel recuperator (FR) and the pre-reformer (PR) where 30% fuel is pre-reformed by mixing with steam extracted from the ST of the bottoming cycle at the desired pressure. A PR is used because in SOFC integrated power systems, often partial reforming is done to avoid problems associated with entrance region local sub-cooling, inhomogeneous temperature distributions, thermal stress and anode carbon deposition etc. Reforming of remaining 70% fuel takes place internally within the SOFC; the left over steam from the PR and the heat of the exothermic electrochemical reaction is the heat source for internal reforming of methane in the SOFC. Some additional amount of fuel flows directly into the combustor (by-passing the

FR, PR and the SOFC) which is burnt along with the SOFC off residual fuels (hydrogen, methane and carbon monoxide) and excess air.

The heat generated during the electrochemical reaction is also used for heating the gaseous stream in the SOFC. The amount of steam extracted for mixing with the fuel prior to its entry to the PR is taken as 2.5 times of the fuel flow rate (FFR), a usual value of steam to carbon (S/C) ratio considered in most of the analyses. Similarly the air stream is compressed in the air compressor (AC) and then preheated in the air recuperator (AR) before it is fed into the SOFC cathode. Unlike the compressed fuel stream, no air can by-pass the SOFC i.e. the whole compressed air stream pass through the SOFC via the AR; this is done to keep the stack temperature at lower level as it will assist in cell cooling. The products of combustion leaving the combustor at high pressure are expanded in the GT. Part of the mechanical work produced by the GT is used to drive the AC and the FC and the remainder is the GT power available for electric power generation. GT exhaust gases are utilized for air and fuel preheating in the FR and AR subsequently. The exhaust gases leaving the AR are further utilized for steam generation in the heat recovery steam generator (HRSG). The steam produced in the HRSG is expanded in the steam turbine (ST) for further production of power. Some amount of steam is extracted for mixing with the fuel prior to its entry to the PR of the topping cycle. The pressure of steam extracted varies with compressor pressure ratio (CPR). The remaining steam is expanded in the ST to the condenser pressure. The expanded steam is then condensed in the condenser before pumping to the HRSG. Both energy and exergy based performances of the proposed cycle are studied based on its variation with CPR. Further a performance comparison is made with a similar other system with AR ahead of FR (ARAOFR).

3.3 System modeling and assumptions

Modeling of the various system components is presented in the following sections. The assumptions made in the model are: (i) steady state system operation; (ii) identical cells in the SOFC stack; (iii) adiabatic cells with negligible heat loss to the surrounding; (iv) ideal gas model for anode, cathode and combustion gases; (v) same temperature of anode and cathode exit stream (vi) Negligible potential and kinetic energy effect (vii) Reference environment temperature 298.15 K and pressure 1 atm. (viii)

Negligible chemical and thermo-mechanical exergy of incoming air and negligible fuel thermo-mechanical exergy.

3.4 Topping SOFC–GT cycle

3.4.1 SOFC electrochemical model

Electrochemical modeling of a fuel cell is about determining the reversible cell voltage, cell over-potentials (losses), actual cell voltage and the cell power. Fuel cell electrochemical performance mainly depends upon factors such as fuel and air utilization, composition of electrode streams, partial pressure and temperature of anode and cathode gases, fuel cell component material and geometry etc.

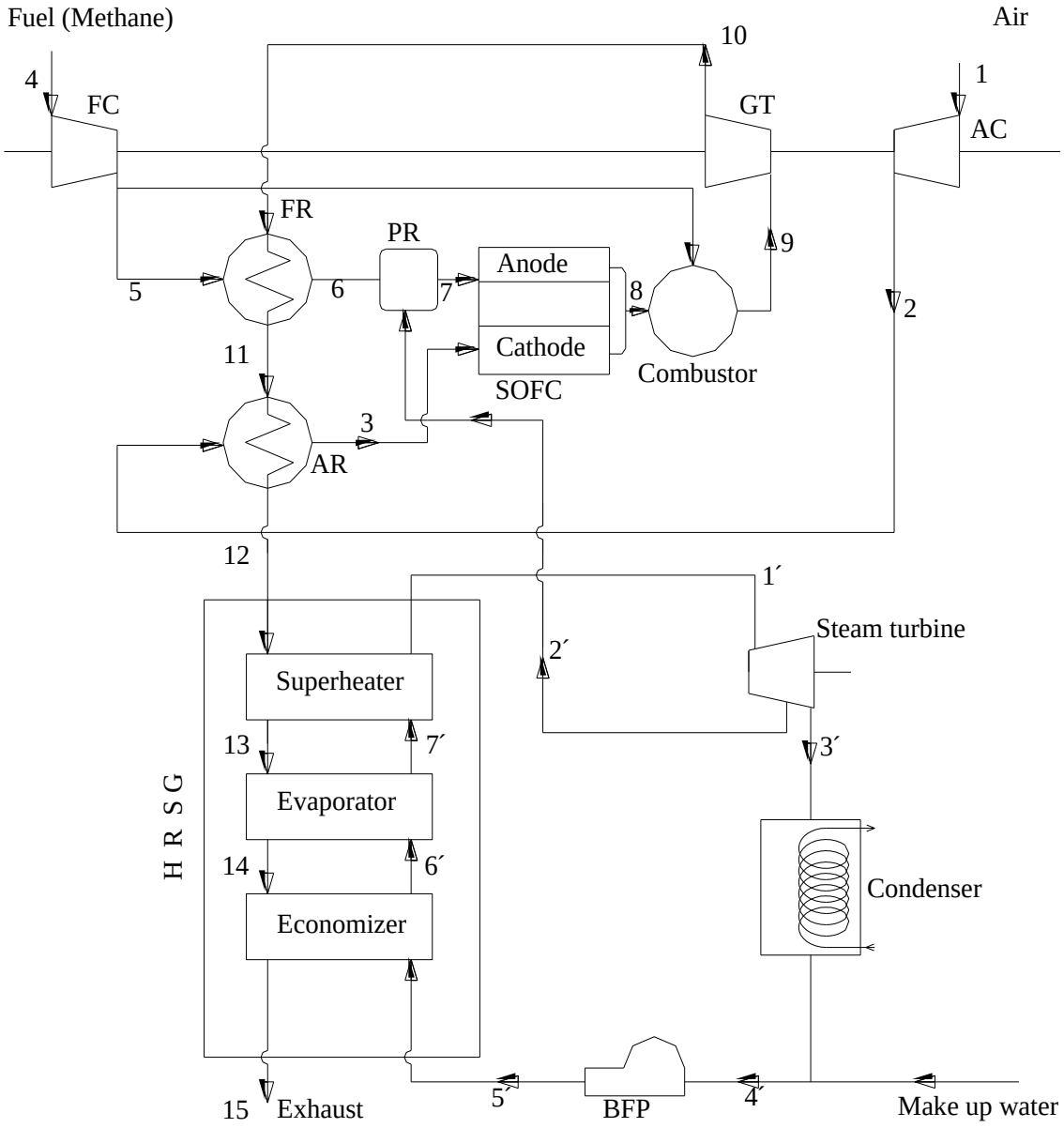

Fig. 3.1: Schematic of the hybrid SOFC–GT–ST power system

The reversible open-circuit voltage of a single fuel cell is calculated from the Nernst equation [7, 8].

$$E = \frac{-\Delta G^0}{2F} + \frac{RT}{2F} \ln \frac{p_{H_2} p_{O_2}^{1/2}}{p_{H_2O}} \tag{3.1}$$

Actual voltage is the reversible open circuit voltage minus the cell over-potentials (ohmic, activation, concentration).

$$V = E - \left(V_{ohm} + V_{act} + V_{conc}\right) \tag{3.2}$$

(1) Ohmic over-potential: Ohmic over-potential is calculated as [9]:

$$V_{ohm} = i\sum \rho_j l_j \tag{3.3}$$

with $\rho_j = A_j \exp\left(\frac{B_j}{T}\right)$, The values of the coefficients A_j and B_j of specific resistivity ρ and the thickness l of the SOFC components are given in Table 3.1 [9, 10]. This is valid for cathode supported SOFC (Ni-YSZ).

Table 3.1: Resistivity constants and thickness of SOFC components

	A(ohm-cm)	B(K)	l (cm)
Anode	0.00298	-1392	0.015
Cathode	0.008114	600	0.2
Electrolyte	0.00294	10350	0.004
Interconnect	0.1256	4690	0.01

(2) Activation over-potential: The Butler–Volmer equation is used to calculate the activation loss [11, 12].

$$i = i_{0,electrode}\left\{\exp\left(\beta\frac{n_e F V_{act,electrode}}{RT}\right) - \exp\left(-(1-\beta)\frac{n_e F V_{act,electrode}}{RT}\right)\right\} \tag{3.4}$$

In equation (3.4), i_0 is the exchange current density, β is the transfer coefficient, F is the Faraday constant ($96{,}485\times10^3$ c/kmol) and n_e is the number of electrons (2 in the present study). The transfer coefficient β is a representative of the cell potential promoting the cell electrochemical reaction and its value is usually taken as 0.5 [9, 11]. The exchange current density i_0 is an important electrochemical kinetics parameter that represents the equilibrium current density at zero net current with zero activation polarization. Higher the value of exchange current density, faster the electrochemical reaction rate and better the fuel cell performance.

For $\beta = 0.5$, the activation polarizations for the electrodes can be written as

$$V_{act,electrode} = \frac{2RT}{n_e F} \sinh^{-1}\left(\frac{i}{i_{0,electrode}}\right) \tag{3.5}$$

Expressions for anode and cathode exchange current density are taken from reference [11].

$$i_{0,an} = \gamma_{an}\left(\frac{p_{H_2}}{p_{ref}}\right)\left(\frac{p_{H_2O}}{p_{ref}}\right)\exp\left(\frac{-E_{act,an}}{RT}\right) \tag{3.6}$$

$$i_{0,ca} = \gamma_{ca}\left(\frac{p_{O_2}}{p_{ref}}\right)^{0.25}\exp\left(\frac{-E_{act,ca}}{RT}\right) \tag{3.7}$$

E_{act}, in the above two equations is the activation energy. Anode and cathode activation energy values are taken as 100×10^6 J/kmol and 120×10^6 J/kmol respectively [11]. The pre-exponential factors for the anode $(\gamma_{an})$and cathode(γ_{ca}) respectively are 5.5×10^4 A/cm^2 and 7.0×10^4 A/cm^2[11].

(3) Concentration over-potential: Consumption of hydrogen and oxygen in the respective electrode-electrolyte interface causes concentration gradient of the reactants and voltage loss i.e. known as concentration over potential. The following equations are used for calculation of concentration over-potential at the anode and cathode and these are taken from References [11,13]. The calculation is done by considering porous electrode structure such as porosity, tortuosity, pore radius and mass transport in the porous electrodes through use of ordinary binary and Knudsen diffusion. Same values of porosity and tortuosity are taken for the anode and cathode; electrode porosity and tortuosity are taken as 0.5 and 3 respectively. The average pore radius is taken as 0.5 μm [11].

$$V_{conc,\,an} = -\frac{RT}{2F}\ln\left[\frac{(1-\left(\frac{RT}{2F}\right)\left(\frac{l_{an}}{D_{an(eff)}P^I_{H_2}}\right)i}{(1+\left(\frac{RT}{2F}\right)\left(\frac{l_{an}}{D_{an(eff)}P^I_{H_2O}}\right)i}\right] \tag{3.8}$$

$$V_{conc,ca} = -\frac{RT}{4F}\ln\left[\frac{\left(\frac{p_{ca}}{\delta_{O_2}}\right)-\left(\left(\frac{p_{ca}}{\delta_{O_2}}\right)-p^I_{O_2}\right)\exp\left[\left(\frac{RT}{4F}\right)\left(\frac{\delta_{O_2} l_{ca}}{D_{ca(eff)}p_{ca}}\right)i\right]}{p^I_{O_2}}\right] \quad (3.9)$$

$D_{an(eff)}$, $D_{ca(eff)}$ in the above equations are the anode and cathode effective diffusion coefficient. $D_{an(eff)}$ is calculated by solving the following quadratic equation[14]

$$D^2{}_{an(eff)} - \left[\left(\frac{p^I_{H_2O}}{p_{an}}\right)D_{H_{2(eff)}} + \left(\frac{p^I_{H_2}}{p_{an}}\right)D_{H_2O_{(eff)}}\right]D_{an(eff)} - \frac{RTl_{an}i}{2Fp_{an}}\left(D_{H_2(eff)} + D_{H_2O(eff)}\right) = 0 \quad (3.10)$$

$$\text{Where, } D_{H_2(eff)} = \left(\frac{\varepsilon}{\zeta}\right)\times\left(\frac{D_{H_2,k}\times D_{H_2-H_2O}}{D_{H_2,k}+D_{H_2-H_2O}}\right) \quad (3.11)$$

$$D_{H_2O(eff)} = \left(\frac{\varepsilon}{\zeta}\right)\times\left(\frac{D_{H_2O,k}\times D_{H_2-H_2O}}{D_{H_2O,k}+D_{H_2-H_2O}}\right) \quad (3.12)$$

Equations (3.13) and (3.14) are used for calculating the Knudsen diffusion coefficients ($D_{H_2,k}$ and $D_{H_2O,k}$) the ordinary binary diffusion coefficient ($D_{H_2-H_2O}$) respectively.

$$D_{A,k(eff)}) = \left(\frac{\varepsilon}{\zeta}\right)\times 97\bar{r}\sqrt{\frac{T}{M_A}} \quad (3.13)$$

where ε and ζ are the porosity and tortuosity and M is the molecular mass. $\bar{r}$ is the average pore radius.

$$D_{AB(eff)} = \left(\frac{\varepsilon}{\zeta}\right)\times 0.0018583\left(\frac{1}{M_A}+\frac{1}{M_B}\right)^{\frac{1}{2}}\frac{T^{3/2}}{p\sigma_{AB}{}^2\Omega_{DAB}} \quad (3.14)$$

In equation (3.14), Ω_{DAB} is the collision integral based on Lennard Jones potential which is obtained from the energy of molecular interaction [13]. σ_{AB} is the collision diameter which is computed by averaging the molecular radii of each species. With reference to equation (3.9),

$$\delta_{O_2} = \left(\frac{D_{O_2,k(eff)}}{D_{O_2,k(eff)} + D_{O_2-N_2(eff)}} \right) \tag{3.15}$$

3.4.2 SOFC thermodynamic model

The reactions that occur in an SOFC stack are well known.

$$x\left(CH_4 + H_2O \leftrightarrow CO + 3H_2\right) \text{ (Reforming)} \tag{3.16}$$

$$y\left(CO + H_2O \leftrightarrow H_2 + CO_2\right) \text{ (Shifting)} \tag{3.17}$$

$$z\left(H_2 + \frac{1}{2}O_2 \leftrightarrow H_2O\right) \text{ (Electrochemical)} \tag{3.18}$$

where, *x*, *y* and *z* indicate respective molar flow rate in the reactions. The equilibrium constants for the reforming $\left(K_{pr}\right)$and shifting reaction$\left(K_{ps}\right)$in terms of the partial pressure and molar concentration of the reactants and the products can be expressed as follows.

$$K_{pr} = \frac{p_{H_2}^3 p_{CO}}{p_{CH_4} p_{H_2O}} = \frac{x_{H_2}^3 x_{CO}}{x_{CH_4} x_{H_2O}} \left(p_{cell}\right)^2 = \frac{\left(H_2^i + 3x + y - z\right)^3 \left(CO^i + x - y\right)}{\left(CH_4^i - x\right)\left(H_2O^i - x - y + z\right)\left(n_{tot}^i + 2x\right)} \left(p_{cell}\right)^2 \tag{3.19}$$

$$K_{ps} = \frac{p_{H_2} p_{CO_2}}{p_{CO} p_{H_2O}} = \frac{x_{H_2} x_{CO_2}}{x_{CO} x_{H_2O}} = \frac{\left(H_2^i + 3x + y - z\right)\left(CO_2^i + y\right)}{\left(CO^i + x - y\right)\left(H_2O^i - x - y + z\right)} \tag{3.20}$$

H_2^i, CO^i, CH_4^i etc. are initial molar concentration of the respective gases. n_{tot}^i in the above equations is the sum of initial molar concentrations of the gases.

The hydrogen utilized in the fuel cell can be defined as follows:

$$z = U_f \left(H_2^i + 3x + y\right) \tag{3.21}$$

The equilibrium constant as polynomial function of temperature [11, 15, 16] is expressed as follows.

$$\log K_p = AT^4 + BT^3 + CT^2 + DT + E \tag{3.22}$$

The values of the constants in equation (3.22) for the reforming and the shifting reactions are known [11, 15, 16] and the equilibrium constants (K_{pr}, K_{ps}) at any given temperature can be found out.

With known values of K_{pr}, K_{ps} and U_f and then by replacing *z* in equations (3.19) and (3.20) we obtain two algebraic equations of the form as given below.

$$a_1x^4 + a_2y^4 + a_3x^3y + a_4xy^3 + a_5x^2y^2 + a_6x^3 + a_7y^3 + a_8x^2y + a_9xy^2 + a_{10}x^2 + a_{11}y^2 + a_{12}xy + a_{13}x + a_{14}y + a_{15} = 0 \quad (3.23)$$

$$b_1x^2 + b_2y^2 + b_3xy + b_4x + b_5y + b_6 = 0 \quad (3.24)$$

The values of the coefficients 'a_i's with $i = 1,2,...,15$ are found in terms of K_{pr}, p, N_{tot}^i, U_f and initial molar concentration of the species. Similarly, the values of the coefficients 'b_i's with $i = 1,2,...,6$ are evaluated based on known values of K_{ps}, U_f and initial molar concentration of the species.

Equations (3.23) and (3.24) are solved for *x* and *y* using Newton's method and then *z* is calculated using Equation (3.21).

The reforming reaction is endothermic while the shifting and the electrochemical reactions are exothermic. The heat of reactions involved in the reforming and shifting reaction can be calculated using Equations (3.25) and (3.26) respectively [10].

$$Q_r = x\left(h_{CO} + 3h_{H_2} - h_{H_2} - h_{CH_4}\right) \quad (3.25)$$

$$Q_s = y\left(h_{CO2} + h_{H_2} - h_{CO} - h_{H_2O}\right) \quad (3.26)$$

$$Q_{rxn} = I\left(V_{ohm} + V_{act} + V_{conc}\right) + T\Delta S \quad (3.27)$$

$$\text{where, } \Delta S = S^0_{H_2O} - S^0_{H_2} - S^0_{O_2} - \frac{R}{2}\ln\left(\frac{p^2_{H_2}\, p_{O_2}}{p^2_{H_2O}}\right) \quad (3.28)$$

The molar specific enthalpy (h) and entropy (S) of the species is determined considering these to be function of temperature [16]. Q_{rxn} is the amount of heat generated during electrochemical reaction. The reversible reaction and the process irreversibility associated with cell polarization are the two main source of Q_{rxn} which is

expressed in the form as stated in equation (3.27) [10]. It is assumed that the heat required for the reforming is supplied from Q_{rxn} [11] and the net heat available is calculated using equation (3.29). The net heat generated in the fuel cell heats the gases in the anode and cathode stream to the stack temperature (T_S) which is calculated iteratively applying heat balance to the SOFC stack. Initially its value is guessed, then the following two terms are calculated.

$$Q = Q_{rxn} + Q_s - Q_r \tag{3.29}$$

$$Q' = \left(\dot{n}_1 \int_{T_{an}}^{T_s} C_p dT \right)_r + \left(\dot{n}_1 \int_{T_{an}}^{T_s} C_p dT \right)_p + \left(\dot{n}_2 \int_{T_{ca}}^{T_s} C_p dT \right)_r + \left(\dot{n}_2 \int_{T_{ca}}^{T_s} C_p dT \right)_p \tag{3.30}$$

In Equation (3.30), T_{an} and T_{ca} are the anode and cathode inlet temperatures respectively. $\dot{n}_1$, $\dot{n}_2$, $\dot{n}_3$ and $\dot{n}_4$ are the corresponding molar flow rates of the gases. Molar specific heat, C_p for the gases are considered temperature dependent. Then iteration is continued until the convergence criterion is met. The convergence criterion is set as [10]:

$$Q_{error} = \left| \frac{Q' - Q}{Q} \right| \leq 0.5\% \tag{3.31}$$

The total current (I) and the electric power $(Power_{sofc})$produced by the SOFC can finally be calculated as follows.

$$I = 2Fz \tag{3.32}$$

$$Power_{sofc} = VI \tag{3.33}$$

3.4.3 Modeling of other sub-systems of the topping cycle

Since it is intended to simulate the overall hybrid SOFC–GT–ST system, therefore, system modeling would be incomplete without modeling of the other sub-systems. Component wise modeling of all other topping cycle components is described in the following subsections.

3.4.3.1 Modeling of Compressors

The temperature of air and fuel at the AC and FC exit and their power requirement are determined using the model equations of Bavarsad [11]. First the temperatures at AC and FC outlet are determined from the following equations.

$$\int_1^2 C_{p,a}\frac{dT}{T} = \frac{R}{\eta_{s,AC}}\ln(CPR)_{AC} \tag{3.34}$$

$$\int_4^5 C_{p,CH_4}\frac{dT}{T} = \frac{R}{\eta_{s,FC}}\ln(CPR)_{FC} \tag{3.35}$$

where, $\eta_{s,AC}$ and $\eta_{s,FC}$ are the isentropic efficiencies of the AC and FC respectively.

Next the power required for driving the two compressors are calculated using the following equations.

$$\dot{W}_{AC} = \dot{n}_a \int_1^2 C_{p,a}dT \tag{3.36}$$

$$\dot{W}_{FC} = \dot{n}_f \int_4^5 C_{p,CH_4}dT \tag{3.37}$$

where, $\dot{n}_a$ and $\dot{n}_f$ are the molar flow rate of air and fuel respectively

The molar specific heats of air $(C_{p,a})$ and fuel (C_{p,CH_4}) are considered temperature dependent as defined below.

$$\frac{C_p}{R} = a_1 + a_2T + a_3T^2 + a_4T^3 + a_5T^4 \tag{3.38}$$

The values of the coefficients a_1, a_2, a_3, a_4 and a_5 for air and fuel are given in Table 3.2. Initial fuel and air inlet pressure and temperature are assumed same at 1 atm. and 298.15 K.

Table 3.2: Values of the coefficients used in Equation (3.38) for calculation of molar specific heat of air and fuel

Coefficients	Air	Fuel (methane)
a_1	3.653	3.826
a_2	-1.34E-03	-3.98E-03
a_3	3.29E-06	2.46E-05
a_4	-1.91E-09	-2.27E-08
a_5	-2.76E-13	6.96E-12

3.4.3.2 Recuperators (AR and FR) and pre-reformer

SOFC operating temperature should be high for better fuel cell operation [9]. Fuel and air therefore are preheated before entering the fuel cell. This is accomplished in the two counter flow heat exchangers. Effectiveness-NTU method is adopted for finding

the temperature of air, fuel and gases at the recuperator outlet. Effectiveness of the recuperators are assumed and inlet temperature and pressures are known a priori. The temperatures of air, fuel and the gases at the recuperator outlet are then calculated.

The PR with 30% fuel conversion is modeled using the partial pre-reforming reaction taken from reference [11] and accordingly, the concentrations of species at PR outlet are determined from mass balance.

3.4.3.3 Combustor modeling

Fuels for the combustor are additional fuel supplied directly to it and the residual hydrogen, carbon monoxide and methane from the SOFC which are burnt with unutilized oxygen from the SOFC cathode outlet stream. The following are the combustion reactions considered.

$$CH_4 + 2O_2 \rightarrow CO_2 + 2H_2O \tag{3.39}$$

$$H_2 + \frac{1}{2}O_2 \rightarrow H_2O \tag{3.40}$$

$$CO + \frac{1}{2}O_2 \rightarrow CO_2 \tag{3.41}$$

The combustor outlet temperature and burnt gas composition are determined through energy balance and stoichiometry of the combustion reactions of the three fuel components [9]. The combustion gases (CO_2, H_2O, O_2 *and* N_2) are assumed to be an ideal gas mixture. For the molar specific heat and enthalpy of the combustion gases, the following temperature dependent model is adopted [2]. The expression for molar specific heat of the gases is same with that of Equation (3.38). The values of the coefficients ($a_1 - a_6$) are available in JANAF table [17].

$$\frac{h}{RT} = a_1 + \frac{a_2}{2}T + \frac{a_3}{3}T^2 + \frac{a_4}{4}T^3 + \frac{a_5}{5}T^5 + \frac{a_6}{T} \tag{3.42}$$

From known molar rate composition of the combustion products, the total mass flow rate, mass based specific heat and characteristic gas constant of the combustion gases are determined using following equations.

$$\dot{m}_g = \sum_i \dot{n}_i M_i \tag{3.43}$$

$$C_{pg} = \sum_i Y_i \frac{C_{p,i}}{M_i} \tag{3.44}$$

$$R_g = \sum_i Y_i \frac{R}{M_i} \tag{3.45}$$

where, $\dot{n}_i$, Y_i and M_i are the rate form molar composition, mass fraction and molecular weight of the gaseous components.

3.4.3.4 Gas turbine

The GT inlet pressure is known from the assumed values of CPR, pressure losses in the recuperators, combustor and the SOFC. GT outlet pressure is calculated by considering atmospheric pressure of gases at the HRSG exit and the gas side pressure losses in the HRSG, AR and the FR. The turbine expansion ratio (*TER*) which is the ratio of gas pressure at GT inlet and outlet is thus known. The GT outlet temperature and GT power are then calculated [11]. The equation used for calculating the GT outlet temperature and GT power are as follows:

$$\int_9^{10} C_{p,g} \frac{dT}{T} = -R_g \eta_{s,GT} C_{p,g} \ln(TER) \tag{3.46}$$

$$\dot{W}_{GT} = \dot{m}_g C_{pg,av} (T_9 - T_{10}) \tag{3.47}$$

$\eta_{s,GT}$ in the above equation is the isentropic efficiency of the GT.

The net power output from the GT plant is:

$$\dot{W}_{net,GT} = \dot{W}_{GT} - \dot{W}_{ac} - \dot{W}_{fc} \tag{3.48}$$

3.4.4 Irreversibility calculation for the topping cycle components

The exergy destruction (irreversibility) occurring in various components is calculated from the exergy balance equations applied to each system component under the steady state assumption. In the exergy balance study, the potential and kinetic energy effects of the incoming and outgoing gas streams are ignored. Fuel (methane) chemical exergy is obtained from Gibbs energy of formation of fuel components while its thermo-mechanical exergy is considered to be zero at the FC inlet. The state of air entering the AC is close to the reference state, therefore it is assumed that it is in thermal, mechanical and chemical equilibrium with the reference environment and both the thermo-mechanical and chemical contribution to exergy are equal to zero.

Compressor (AC and FC) irreversibility is calculated from the following equation [11]:

$$\dot{I}_c = T_0 \dot{n} \left[\left(\frac{1-\eta_s}{\eta_s} \right) \ln(CPR) \right] \tag{3.49}$$

The irreversibility in the recuperators (AR and FR) is calculated using Eq. (3.50).

$\dot{I}_{AR/FR}$ = Decrease in exergy rate of hot stream − Increase in exergy rate of cold stream (3.50)

In irreversibility calculation of the SOFC, we consider the chemical and the thermo-mechanical exergy of inlet and outlet streams. Chemical exergy of the component 'i' at electrode inlet and exit is calculated as given below [9, 11].

$$\dot{E}x_{ch} = \sum_i \dot{n}_i \left[ex_{ch,i} + RT_0 \ln(X_i) \right] \tag{3.51}$$

Similarly, thermo-mechanical exergy is:

$$\dot{E}x_{tm} = \sum_i \dot{n}_i \left[\bar{h}_i(T) - \bar{h}_i(T_0) - T_0 \left(\bar{s}_i^{\,0}(T) - \bar{s}_i^{\,0}(T_0) \right) - \bar{R} \ln \frac{p}{p_0} \right] \tag{3.52}$$

Total exergy is the sum of the chemical and the thermo-mechanical exergy.

$$\dot{E}x = \dot{E}x_{ch} + \dot{E}x_{tm} \tag{3.53}$$

SOFC irreversibility is thus evaluated as:

$$\dot{I}_{SOFC} = \dot{E}x_3 + \dot{E}x_7 - \dot{E}x_8 - Power_{sofc} \tag{3.54}$$

PR irreversibility:

$$\dot{I}_{PR} = \dot{E}x_6 + \dot{E}x_{2'} - \dot{E}x_7 \tag{3.55}$$

The combustion irreversibility is found from the following exergy balance equation.

$$\dot{I}_{CC} = \dot{E}x_5 + \dot{E}x_8 - \dot{E}x_9 \tag{3.56}$$

GT irreversibility is:

$$\dot{I}_{GT} = T_0 \dot{n}_g R \left[(1-\eta_{s,GT}) \ln(TER) \right] \tag{3.57}$$

3.5 Bottoming ST cycle

In the ST cycle, the pressurized water after the boiler feed pump (BFP) is heated to produce superheated steam in the HRSG. The HRSG consists of the economizer (ECO), evaporator (EVA) and the super-heater (SUP). Energy balance is done in the HRSG for determination of steam generation rate assuming a fixed exhaust gas temperature of 100°C at HRSG exit. Pressure losses in the bottoming cycle components

are however neglected. The average specific heat of the combustion gases entering and leaving the HRSG is calculated and the mass of steam produced in the HRSG is determined from the following equation.

$$\dot{m}_s\left(h_{1'}-h_{5'}\right)=\dot{m}_g C_{pg,av}\left(T_{12}-T_{15}\right) \tag{3.58}$$

The ST power is calculated as follows.

$$\dot{W}_{ST}=\dot{m}_s\left(h_{1'}-h_{2'}\right)+\left(\dot{m}_s-\dot{m}_{s,extracted}\right)\left(h_{2'}-h_{3'}\right) \tag{3.59}$$

where, $\dot{m}_{s,extracted}$ is the mass of steam extracted for mixing with fuel prior to its entry to the PR. The net power output from the ST plant is:

$$\dot{W}_{net,ST}=\dot{W}_{ST}-\dot{W}_{pump} \tag{3.60}$$

3.5.1 Irreversibility calculation for the bottoming cycle components

ST irreversibility:

$$\dot{I}_{ST}=\dot{m}_s T_0\left(s_{2'}-s_{1'}\right)+\left(\dot{m}_s-\dot{m}_{s,extracted}\right)T_0\left(s_{3'}-s_{2'}\right) \tag{3.61}$$

Condenser irreversibility:

$$\dot{I}_{COND}=T_0\left[\dot{m}_w C_{pw}\log\left(\frac{T_{w,out}}{T_{w,in}}\right)+\left(\dot{m}_s-\dot{m}_{s,extracted}\right)\left(s_{3'}-s_{4'}\right)\right] \tag{3.62}$$

Irreversibility in BFP:

$$\dot{I}_{BFP}=\left(\dot{m}_s-\dot{m}_{s,extracted}\right)T_0\left(s_{5'}-s_{4'}\right) \tag{3.63}$$

3.6 Exhaust irreversibility and efficiency calculation

Exergy destroyed with the exhaust gases is calculated adding the chemical and the thermo-mechanical exergy of exhaust gas stream at the HRSG outlet.

The first law (energy) and second law (exergy) efficiency of the overall system are calculated using the following equations.

$$\eta_I=\frac{Power_{sofc}+\left(\dot{W}_{net,GT}+\dot{W}_{net,ST}\right)\times\eta_{gen}}{\dot{n}_{CH_4}\times LHV} \tag{3.64}$$

$$\eta_{II}=\frac{Power_{sofc}+\left(\dot{W}_{net,GT}+\dot{W}_{net,ST}\right)\times\eta_{gen}}{\dot{n}_{CH_4}\times ex_{CH_4}} \tag{3.65}$$

where, *LHV* is lower heating value and η_{gen} is the generator efficiency. $\dot{W}_{net,GT}$ is the net power of the GT plant given by the following equation. ex_{CH_4} is the molar specific chemical exergy of methane taken as 830174.37 kJ/kmol.

$$\dot{W}_{net,GT} = \dot{W}_{GT} - \left(\dot{W}_{AC} + \dot{W}_{FC}\right) \tag{3.66}$$

The assumed parameters, efficiency and effectiveness of various system components are shown in Table 3.3.

Table 3.3: Assumed values of parameters

Parameter	Value
Compressor isentropic efficiency	85%
GT isentropic efficiency	85%
Combustor efficiency	95%
Generator efficiency	90%
Recuperator (AR and FR) effectiveness	0.75
Fuel utilization factor	0.85
Oxygen utilization factor	0.25
Steam to carbon ratio	2.5
Recuperator pressure drop (AR and FR)	4%
SOFC pressure drop	4%
Combustor pressure drop	5%
Condition of steam at entry to the ST	Superheated at 600°C
Condenser pressure	0.05 bar

Source: Reference[7] for pressure drop values

3.7 Energy and exergy based performance analyses of the proposed SOFC–CC plant

In this research, the energy and exergy based performance analyses of the proposed hybrid SOFC–GT–ST configuration is performed based on variation of CPR, fuel flow rate (FFR), air flow rate (AFR), current density, boiler pressure, ST inlet temperature (STIT). Parametric study evaluating the effect of CPR and the other parameters on performance of the individual components and particularly the bottoming

ST plant is important in the sense that effect of these parameters on power output from the bottoming ST plant of a combined SOFC–GT–ST plant has not been comprehensively investigated.

Further, investigation is done to study the effect of additional fuel supply to the combustor (by-passing the FR and the SOFC) on power output from the bottoming GT and ST plant considering a single pressure level in the ST cycle to make the analysis simple. This single level boiler pressure was however optimized for maximum power through parametric variation of boiler pressure. The proposed SOFC–GT–ST plant is relatively of bigger size as it has been designed to produce power in the range of 42.7 to 62.1 MW using various options of CPR, FFR, AFR, current density, with and without additional fuel burning, boiler pressure, STIT etc. Moreover, exergy is applied to find out the source of inefficiency and irreversibility of all components of the proposed new SOFC–GT–ST system.

A MATLAB code is developed and used for the system simulation. The main program is linked with individual subroutines written for modeling various system components where mass, energy and exergy balance equations are solved simultaneously. Further, we have made a performance comparison between the proposed system and a similar other system where the AR is placed ahead of the FR (ARAOFR).

3.7.1 Effect of additional fuel burning and CPR on system performance

In combined SOFC–GT–ST system, the bottoming ST plant produces the least power as evident from the work of Arsalis [18]. The fraction of power produced in the GT and ST can be increased through burning of additional fuel in the Combustor/afterburner. In an attempt to increase the power output from the GT and ST plant, compressed additional fuel is supplied to the Combustor to investigate the effect of additional fuel burning on power and efficiency of the combined plant. The flow rate of additional fuel is varied from no additional fuel up to a maximum 50% of the fixed FFR (300 kmol/h) supplied to the SOFC anode. The effect of additional fuel burning on SOFC power, net GT and ST power, total power and energy efficiency are summarized in Table 3.4. With no additional fuel burning in the Combustor, the total power and efficiency of the plant increases from 42.70 MW, 62.87% at CPR 6 to 45.58 MW, 67.07% at CPR 14. It is also observed that the most of the power (in an average 67.2%) is produced by the SOFC; the net GT and ST power sharing only average 25.8% and

7.5% of the total power respectively. Moreover, at higher CPR, the SOFC power and net GT power increases while the net ST power reduces. With burning of additional fuel, both the GT and ST power increases gradually. It was observed that burning of 50% additional fuel in the combustor causes significant increase in the GT and ST power values, more than double in case of the net ST power at all CPR. But at the same time the TIT also increases which in turn may demand use of costly GT blade materials. But with the development of new advanced materials, TIT of the order of 1743–1753 K may be possible. SOFC power reduces slightly with increasing amount of additional fuel supply to the combustor; however this is not due to additional fuel burning. Actually with increase in additional fuel, the air supply to the SOFC cathode is also increased to provide the excess air required for burning the additional fuel in the combustor. It results in cell cooling which is evident from the lower stack temperatures shown in the table. The SOFC power in this case has decreased due to reduction in the stack temperature; the SOFC stack temperature reduces by about 22°C at CPR 14 when airflow rate is increased from 3500 kmol/h to 5000 kmol/h along with increase in additional fuel supply from 0 to 150 kmol/h. Further, it is seen that with no additional fuel burning, the SOFC stack temperature reduces with CPR. At higher CPR, the SOFC operating pressure increases causing changes in the partial pressure of the constituent gases and the equilibrium of the reforming, shifting and electrochemical reactions. At higher pressure, the cell over-potential and the heat released during the electrochemical reaction also reduces causing a reduction in the SOFC stack temperature. This is the case when no additional fuel is burnt in the combustor, but with increase in the amount of additional fuel burning this reducing trend gradually vanishes. Actually the SOFC power increases along with the GT and ST power due to additional fuel burning with fixed amount of air. This was checked in this study and we found power values of 31.66 MW, 16.99 MW and 3.69 MW respectively from the SOFC, the GT and the ST plant at CPR 14 with 50 kmol/h of additional fuel against 30.42 MW, 12.48 MW and 2.69 MW without additional fuel while keeping the AFR constant at 3500 kmol/h. As we can see, the GT and ST power in that case shows significant gain particularly the GT power with an overall 14.82% gain in total power. But the efficiency anyhow reduces (in this case from 67.07% to 65.79% at CPR 14); this is because SOFC is an efficient electrochemical energy conversion device; burning of some additional amount of fuel in the combustor bypassing the SOFC causes this reduction in efficiency. The results shown in Table 3.4

correspond to boiler pressure of 40 bar with superheated steam temperature of 600°C at ST inlet.

Variation of irreversibility in the system components with CPR is shown in Figs. 3.2–3.4. It is seen that the irreversibility in the SOFC, combustor, HRSG, PR, AR, BFP and the condenser reduces with increase in CPR. The components in which the irreversibility increases with CPR include the GT, FR, AC and the FC. Irreversibility in these components increases with CPR due to more entropy generation at higher pressure. The FR irreversibility increases during CPR variation up to CPR 12 but it then falls down again at CPR 14. On the other hand, the ST irreversibility initially decreases and then again increases with increase in CPR value. The minimum ST irreversibility was registered at CPR value of 8. The exhaust exergy loss also increases with increase in CPR (Fig. 3.4). But overall the total system irreversibility decreases with increasing CPR. The energy and exergy efficiency variation with CPR for the proposed cycle with 50% additional fuel burning is shown in Fig. 3.5. The energy efficiency values for this case at various CPR were shown previously in Table 3.4. Now from Fig. 3.5 it is observed that the exergy efficiency is lower than its corresponding energy efficiency at all CPR and both these efficiencies increase with CPR mainly due to increase in SOFC power and net GT work at higher pressure ratios. The ST power however reduces with increase in CPR.

Table 3.4: System performance variation with CPR and additional fuel burning at 40 bar boiler pressure

$\dot{n}_f$ (kmol/h)	$\dot{n}_{f,add}$ (kmol/h)	$\dot{n}_{air}$ (kmol/h)	Parameter	CPR				
				6	8	10	12	14
300	0	3500	SOFC power (MW)	29.11	29.62	30.02	30.27	30.42
			Net GT power (MW)	10.01	11.11	11.73	12.16	12.48
			Net ST power (MW)	3.58	3.22	3.00	2.83	2.69
			Total power (MW)	42.70	43.96	44.75	45.25	45.58
			stack temperature (K)	1015	1011	1009	1007	1005
			TIT (K)	1399.5	1395.8	1394.4	1393.1	1392.1
			Energy efficiency (%)	62.87	64.70	65.85	66.59	67.07
300	50	4000	SOFC power (MW)	28.36	29.06	29.46	29.70	29.93
			Net GT power (MW)	12.75	14.32	15.32	15.95	16.44
			Net ST power (MW)	4.86	4.46	4.17	3.98	3.83
			Total power (MW)	45.98	47.84	48.96	49.62	50.20
			stack temperature (K)	1007	1005	1003	1001	1000
			TIT (K)	1540.7	1539.8	1539.0	1538.3	1538.8
			Energy efficiency (%)	57.84	60.15	61.54	62.36	63.08
300	100	4500	SOFC power (MW)	27.25	28.06	28.56	28.88	29.11
			Net GT power (MW)	15.47	17.43	18.70	19.60	20.23
			Net ST power (MW)	6.13	5.67	5.36	5.14	4.96
			Total power (MW)	48.85	51.16	52.61	53.62	54.30
			stack temperature (K)	996	995	994	993	992
			TIT (K)	1653.1	1653.7	1654.4	1655.1	1656.0
			Energy efficiency (%)	53.61	56.12	57.69	58.78	59.52
300	150	5000	SOFC power (MW)	25.65	26.73	27.34	27.78	28.10
			Net GT power (MW)	18.09	20.46	22.01	23.16	23.93
			Net ST power (MW)	7.38	6.88	6.53	6.29	6.11
			Total power (MW)	51.12	54.07	55.89	57.22	58.14
			stack temperature (K)	982	983	983	983	983
			TIT (K)	1743.5	1746.4	1748.5	1750.5	1752.7
			Energy efficiency (%)	49.72	52.57	54.32	55.61	56.49

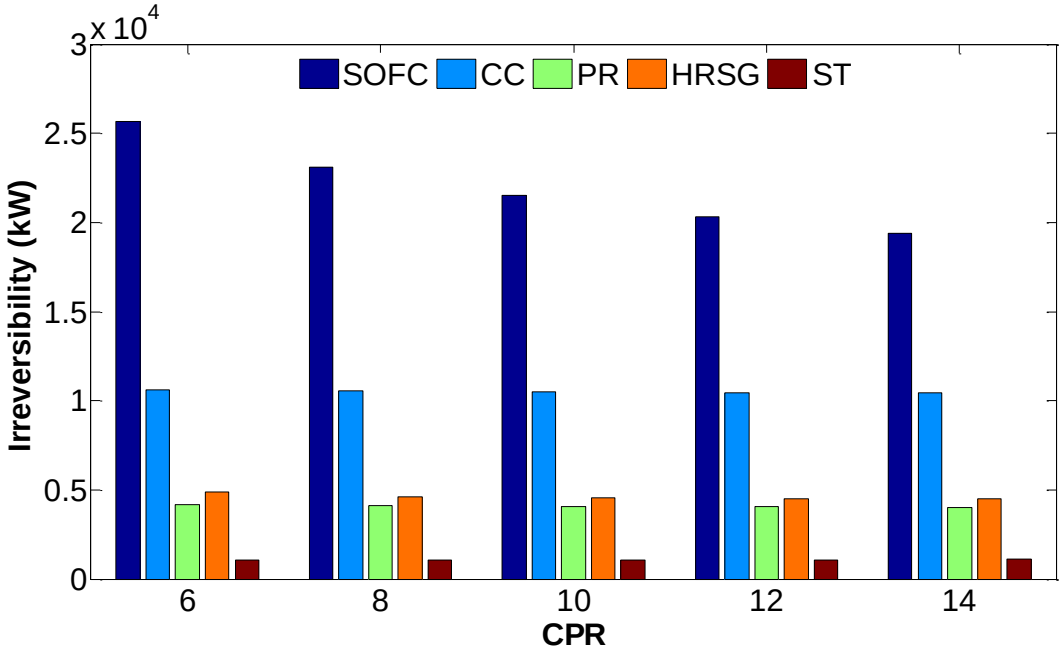

Fig.3.2: Effect of CPR on SOFC, combustor, PR, HRSG and ST irreversibility with 50% additional burning in the combustor at 40 bar boiler pressure.

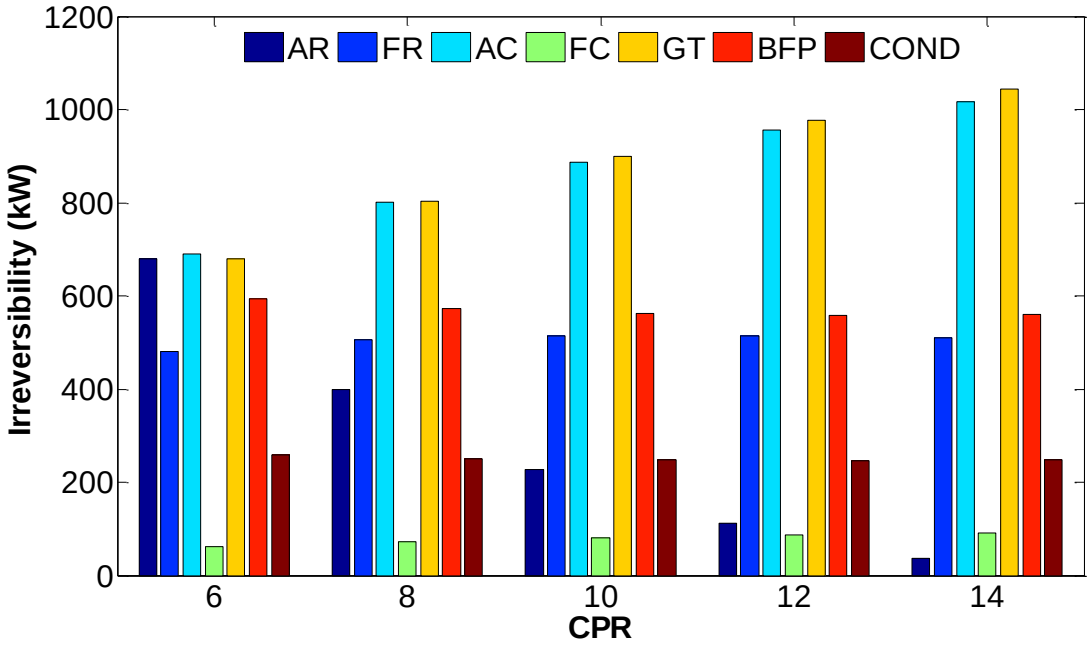

Fig.3.3: Effect of CPR on irreversibility of other system Components with 50% additional burning in the combustor at 40 bar boiler pressure.

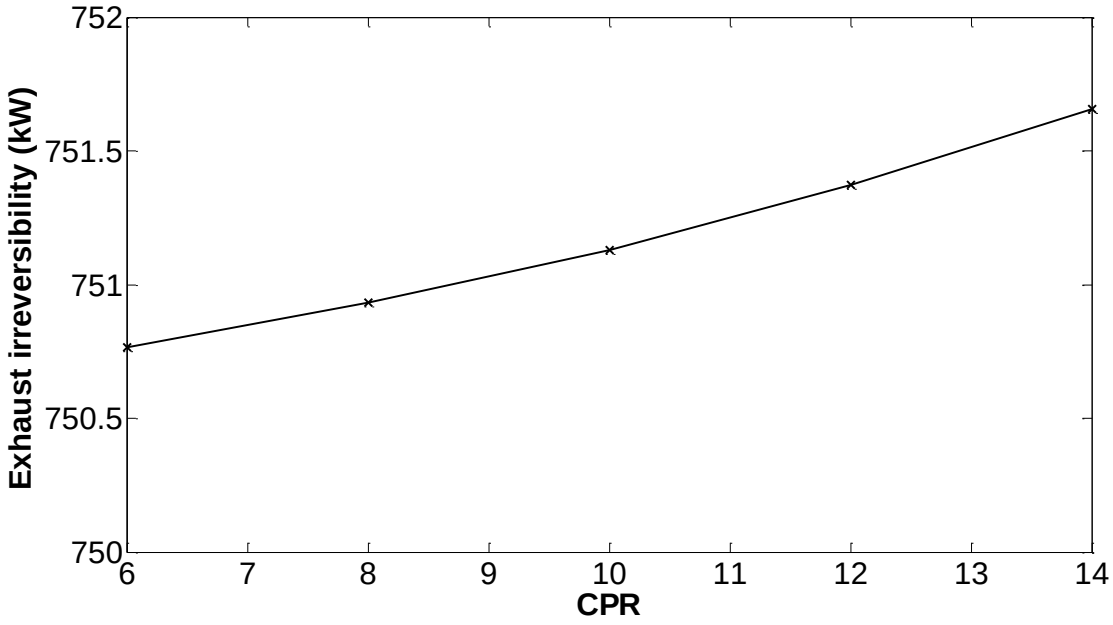

Fig. 3.4: Effect of CPR on exhaust irreversibility with 50% additional burning in the combustor at 40 bar boiler pressure.

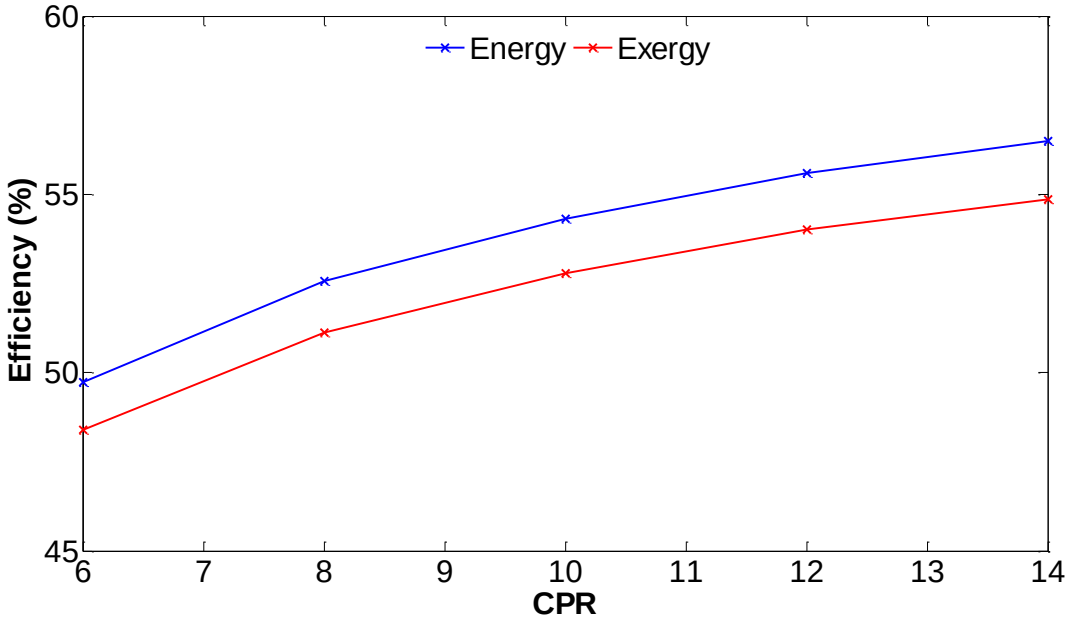

Fig. 3.5: Effect of CPR on energy and exergy efficiency of the hybrid SOFC– GT–ST System with 50% additional burning in the combustor at 40 bar boiler pressure .

3.7.2 Effect of single level boiler pressure on system performance

Since we considered a single level boiler pressure for steam generation in the HRSG and power recovery from the bottoming ST plant, so definitely a question arises as to what boiler pressure provides the maximum power from the ST plant under a given set of operating conditions. Therefore, a parametric study was carried to investigate the effect of the single level boiler pressure on power production from the GT plant, ST plant and the component irreversibility. Detail power results corresponding to single level boiler pressure variation are shown in Table 3.5. Keeping the ST inlet superheated steam temperature fixed at 600°C, when the boiler pressure was varied, the net power obtained from the bottoming ST plant and the total power was found to be the maximum at a boiler pressure of 40 bar. As the boiler pressure exceeds 40 bar, the SOFC power, net GT and ST power all show a decreasing trend. Hence, a boiler pressure of 40 bar was chosen for the steam generation in the HRSG with 50% additional fuel.

The effect of boiler pressure on component irreversibility is shown in Table 3.6. With change in boiler pressure, irreversibility changes take place in the PR and the bottoming ST cycle components. Irreversibility in the topping SOFC–GT cycle components and the exhaust exergy loss are not affected much due to boiler pressure variation. Irreversibility in the HRSG increases slightly during boiler pressure variation from 35 to 60 bar and decreases thereafter with significant reduction at higher boiler pressure. ST, condenser and BFP irreversibility increases with boiler pressure; HRSG irreversibility is the maximum among them. Irreversibility in the PR also increases slightly with increase in boiler pressure. Hence, the total system irreversibility increases with increase in boiler pressure. Component wise, the maximum irreversibility occurs in the SOFC of the topping SOFC–GT cycle. Irreversibility in the SOFC occurs mainly due to the electrochemical and the other reactions which are highly irreversible in nature. Next major contributor of system irreversibility is the combustor. Irreversibility in the combustor occurs due to the combustion reactions at high temperature that are highly irreversible. Irreversibility in other system components is comparatively less. Among these, the irreversibility in the HRSG is the highest followed by irreversibility contribution by the PR, ST, GT, AC, exhaust gases, BFP, FR, Condenser, FC and the AR.

3.7.3 Effect of FFR on system performance

The effect of FFR on system performance and component irreversibility is presented in Table 3.7. With increase in FFR, the cell over-potential decreases due to increase in the SOFC stack temperature hence the cell voltage is more at higher FFR. Keeping fuel utilization factor constant when FFR is increased, more chemical energy is available for conversion into electrical and thermal energy and hence, the current production and heat generation during the electrochemical reaction increases. This in turn increases the power production in the SOFC stack and the SOFC stack temperature. This would further increase the TIT through burning of the additional and residual fuels in the combustor. Hence, the GT would be able to produce more power due to expansion of high temperature gases through a fixed TER. Proportionally, the FC power requirement will also increase, however comparatively greater increase in the GT power will finally lead to an increase in the net GT power output. The ST power also increases due to increase in temperature and mass flow rate of the gases at the HRSG inlet. No doubt, the fuel energy and exergy input will also increase with FFR, however the proportional increase in power in the SOFC, GT and ST would also be more resulting in an increase in the overall system energy and exergy efficiency. Irreversibility in all system components (except the AC) shows an overall increase with FFR. This is mainly due to increase in SOFC stack temperature, TIT and the exhaust gas temperature The irreversibility in the AC is not affected by increase in FFR; hence it remains constant.

Table 3.5: System performance variation with CPR and boiler pressure at CPR 14 with 50% additional fuel burning

P_b (bar)	Power (MW)	CPR				
		6	8	10	12	14
35	SOFC power	25.77	26.73	27.34	27.78	28.10
	Net GT power	18.09	20.46	22.01	23.16	23.93
	Net ST power	7.36	6.85	6.50	6.24	6.06
	Total power	51.22	54.05	55.85	57.17	58.09
40	SOFC power	25.65	26.73	27.34	27.78	28.10
	Net GT power	18.09	20.46	22.01	23.16	23.93
	Net ST power	7.38	6.88	6.53	6.29	6.11
	Total power	51.12	54.07	55.89	57.22	58.14
50	SOFC power	25.65	26.62	27.23	27.66	27.99
	Net GT power	18.10	20.47	22.02	23.10	23.94
	Net ST power	7.27	6.80	6.47	6.24	6.06
	Total power	51.02	53.89	55.72	57.00	57.99
60	SOFC power	25.53	26.50	27.23	27.54	27.87
	Net GT power	18.10	20.41	22.02	23.11	23.89
	Net ST power	7.03	6.57	6.27	6.04	5.87
	Total power	50.66	53.48	55.52	56.69	57.63
70	SOFC power	25.53	26.50	27.11	27.54	27.75
	Net GT power	18.10	20.41	21.96	23.11	23.91
	Net ST power	6.65	6.23	5.94	5.70	5.54
	Total power	50.28	53.14	55.01	56.35	57.20
80	SOFC power	25.40	26.50	26.99	27.42	27.75
	Net GT power	18.11	20.42	21.97	23.05	23.91
	Net ST power	6.14	5.74	5.46	5.24	5.09
	Total power	49.65	52.66	54.42	55.71	56.75
90	SOFC power	25.40	26.38	26.99	27.42	27.63
	Net GT power	18.11	20.42	21.97	23.05	23.85
	Net ST power	5.50	5.12	4.86	4.64	4.49
	Total power	49.01	51.92	53.82	55.11	55.97
100	SOFC power	25.40	26.38	26.99	27.30	27.63
	Net GT power	18.11	20.42	21.97	23.07	23.85
	Net ST power	4.73	4.35	4.11	3.90	3.74
	Total power	48.24	51.15	53.07	54.27	55.22

Table 3.6: Component and total system irreversibility variation with boiler pressure at CPR 14 with 50% additional fuel burning

Irreversibility (MW)	Boiler pressure (bar)							
	35	40	50	60	70	80	90	100
HRSG	4.452	4.508	4.625	4.722	4.712	4.514	3.943	2.657
ST	1.077	1.105	1.163	1.231	1.302	1.384	1.469	1.568
COND	0.243	0.248	0.260	0.275	0.290	0.308	0.328	0.351
BFP	0.450	0.560	0.838	1.222	1.756	2.526	3.673	5.475
PR	4.017	4.026	4.039	4.052	4.066	4.080	4.094	4.103
SOFC	19.459	19.366	19.348	19.392	19.429	19.349	19.438	19.383
Combustor	10.425	10.425	10.429	10.432	10.435	10.435	10.438	10.438
GT	1.043	1.043	1.043	1.043	1.043	1.043	1.043	1.043
FR	0.509	0.509	0.509	0.509	0.509	0.509	0.509	0.509
AR	0.036	0.036	0.037	0.037	0.038	0.038	0.038	0.038
FC	0.091	0.091	0.091	0.091	0.091	0.091	0.091	0.091
AC	1.016	1.016	1.016	1.016	1.016	1.016	1.016	1.016
Exhaust	0.7516	0.7516	0.7516	0.7516	0.7516	0.7517	0.7517	0.7517
Total	43.570	43.685	44.150	44.774	45.439	46.045	46.832	47.424

Table 3.7: Effect of FFR on simulation results

FFR (kmol/h)	280	290	300	310	320
SOFC power (MW)	25.32	26.71	28.10	29.40	30.82
Net GT power (MW)	22.83	23.41	23.93	24.46	25.05
Net ST power (MW)	5.98	6.04	6.11	6.17	6.23
Total power (MW)	54.13	56.16	58.14	60.03	62.10
Stack temperature (K)	975	979	983	986	990
TIT (K)	1741.1	1746.9	1752.7	1757.7	1763.5
Single cell voltage (V)	0.562	0.572	0.582	0.589	0.598
Energy efficiency (%)	55.01	55.79	56.49	57.08	57.81
Exergy efficiency (%)	53.44	54.19	54.87	55.43	56.14
Irreversibility (MW)					
HRSG	4.298	4.398	4.508	4.610	4.713
ST	1.090	1.097	1.105	1.113	1.120
COND	0.246	0.247	0.248	0.249	0.250
BFP	0.555	0.557	0.560	0.563	0.565
PR	3.751	3.887	4.026	4.154	4.290
SOFC	19.364	19.362	19.366	19.491	19.432
Combustor	10.366	10.396	10.425	10.458	10.488
GT	1.028	1.036	1.043	1.051	1.059
FR	0.486	0.498	0.509	0.521	0.533
AR	0.034	0.035	0.036	0.038	0.039
FC	0.087	0.089	0.091	0.093	0.095
AC	1.016	1.016	1.016	1.016	1.016
Exhaust	0.699	0.725	0.752	0.780	0.808
Total Irreversibility	43.020	43.343	43.685	44.137	44.408

3.7.4 Effect of AFR on system performance

AFR is an important parameter, it affects fuel cell stack cooling and thus the SOFC stack temperature and the TIT are directly affected by AFR. The influence of AFR on system performance is illustrated in Table 3.8. Keeping the FFR and other input parameters constant when a AFR is varied the reverse happens i.e. the cell over-potential

increases causing a reduction in the cell voltage. The SOFC stack temperature also decreases due to cell cooling by relatively a larger amount of air. The current produced in the SOFC does not change much with AFR; however since the cell voltage is less, hence the SOFC power decreases with AFR. Due to reduction in stack temperature and consequently the TIT, the GT power also gets reduced when AFR is increased. On the other hand, the AC power requirement increases causing an increase in the total compressor work which finally reduces the net GT power. The ST power however does not change much with increase in AFR and shows slight improvement. Increased AFR thus has negative effect on overall system efficiencies (energy and exergy) because of reduction in SOFC and net GT power. Irreversibility in all the components and the total system irreversibility increases with AFR except in the HRSG, PR and the exhaust gas irreversibility. The irreversibility in the FC is not affected by change in the AFR.

3.7.5 Effect of current density on system performance

For studying the effect of current density on system performance, it is varied from 0.2 A/cm^2 to 0.6 A/cm^2 while keeping the other parameters fixed. The effect of current density on cell voltage, power, system efficiencies and component irreversibility is shown in Table 3.9. The cell voltage decreases with current density due to increase in cell over potential at higher current density [9, 11, 19]. That the cell over-potentials increase with current density is shown in Figs. 3.6 and 3.7. Concentration over-potential contributes very little to the cell voltage loss as compared to the ohmic and activation loss. Increase in current density causes an increase in the stack temperature. This is due to increased voltage loss and higher energy dissipation at higher current density [19] which ultimately leads to higher amount of heat release during the electrochemical reaction. Keeping the FFR fixed when the current density is increased, the SOFC area decreases and also due to lower cell voltage and lower current finally the power produced by the SOFC will also be less at higher current density. However, due to increase in SOFC stack temperature and subsequent burning of the residual fuel in the combustor, the TIT will increase leading to an increase the GT power. The total compressor power however remains invariant with current density, so a gain in the net GT power. Due to increase in SOFC stack temperature and TIT, exhaust gas temperature at HRSG inlet will also increase and more amount of steam is produced in the HRSG. Thus the net ST increases slightly with increase with current density. Although net GT

and ST power increases with current density but the SOFC power decreases significantly, hence the energy and exergy efficiency of the overall system decreases. Irreversibility in various system components increases with current density except in the combustor and AR. AC and FC irreversibility is not affected by changes in current density.

Table 3.8: Effect of AFR on simulation results

AFR (kmol/h)	4500	4725	4950	5175	5400
SOFC power (MW)	29.42	28.78	28.22	27.51	26.88
Net GT power (MW)	24.42	24.24	23.98	23.74	23.55
Net ST power (MW)	6.00	6.04	6.09	6.14	6.19
Total power (MW)	59.84	59.06	58.30	57.39	56.63
Stack temperature (K)	995	989	984	978	973
TIT (K)	1818.4	1787.4	1758.8	1730.9	1705.2
Single cell voltage (V)	0.609	0.596	0.584	0.570	0.5570
Energy efficiency (%)	58.18	57.40	56.65	55.76	55.00
Exergy efficiency (%)	56.49	55.74	55.020	54.16	53.43
Irreversibility (MW)					
HRSG	4.746	4.623	4.528	4.430	4.339
ST	1.084	1.091	1.103	1.113	1.124
COND	0.243	0.245	0.248	0.250	0.253
BFP	0.549	0.553	0.559	0.565	0.571
PR	4.033	4.031	4.023	4.016	4.013
SOFC	18.363	18.858	19.287	19.872	20.325
Combustor	9.921	10.155	10.378	10.595	10.802
GT	0.964	1.000	1.036	1.071	1.107
FR	0.493	0.501	0.508	0.514	0.520
AR	0.014	0.025	0.034	0.045	0.056
FC	0.091	0.091	0.091	0.091	0.091
AC	0.914	0.960	1.006	1.051	1.097
Exhaust	0.799	0.776	0.756	0.739	0.725
Total Irreversibility	42.214	42.909	43.557	44.352	45.023

Table 3.9: Effect of current density on simulation results

Current density (A/cm^2)	0.2	0.3	0.4	0.5	0.6
SOFC power (MW)	30.17	28.10	26.27	24.74	23.53
Net GT power (MW)	23.56	23.93	24.27	24.55	24.79
Net ST power (MW)	6.01	6.11	6.18	6.24	6.31
Total power (MW)	59.73	58.14	56.72	55.53	54.62
Stack temperature (K)	959	983	1000	1014	1027
TIT (K)	1736.5	1752.7	1765.7	1777.0	1787.9
Single cell voltage (V)	0.627	0.582	0.544	0.512	0.487
Energy efficiency (%)	58.11	56.49	55.06	53.85	52.94
Exergy efficiency (%)	56.43	54.87	53.49	52.32	51.44
Irreversibility (MW)					
HRSG	4.390	4.508	4.597	4.675	4.754
ST	1.085	1.105	1.120	1.134	1.147
COND	0.243	0.248	0.252	0.255	0.258
BFP	0.549	0.560	0.569	0.576	0.584
PR	4.018	4.026	4.024	4.027	4.029
SOFC	17.842	19.366	20.740	21.882	22.718
Combustor	10.507	10.425	10.374	10.334	10.299
GT	1.043	1.043	1.043	1.043	1.043
FR	0.508	0.509	0.510	0.510	0.511
AR	0.044	0.036	0.030	0.025	0.019
FC	0.091	0.091	0.091	0.091	0.091
AC	1.016	1.016	1.016	1.016	1.016
Exhaust	0.752	0.752	0.752	0.752	0.752
Total Irreversibility	42.088	43.688	45.118	46.320	47.221

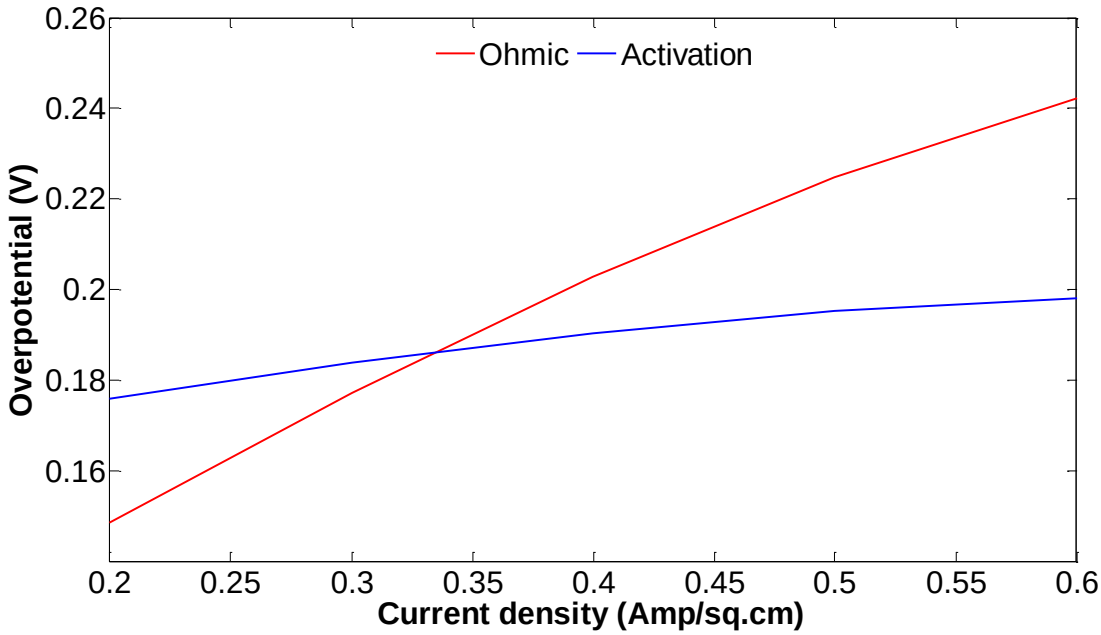

Fig.3.6: Effect of current density on SOFC ohmic and activation overpotential.

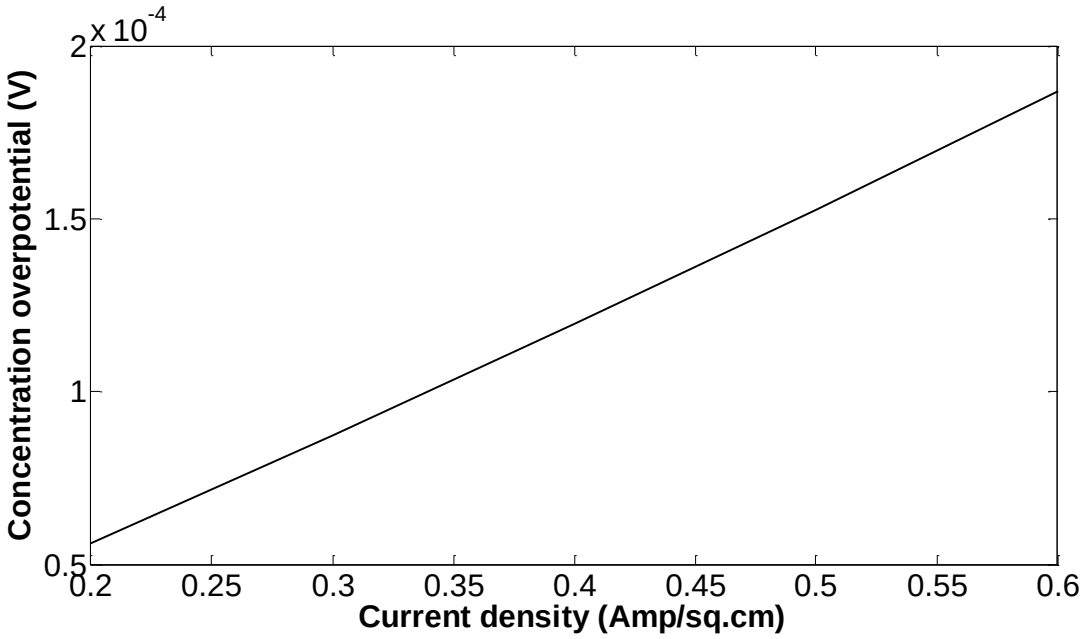

Fig.3.7: Effect of current density on SOFC concentration overpotential.

3.7.6 Effect of STIT on system performance

The temperature of superheated steam at ST inlet was varied from 500°C to 600°C to evaluate its effect on performance and irreversibility of the system components.

Presently the maximum allowable STIT is about 620°C and use of higher STIT demands improvement in material properties or use of new materials that can withstand higher temperatures [20]. As can be seen from Table 3.10, the SOFC power increases marginally by 1.26% while the ST power by 7.76% during STIT variation. There is an overall increase of 1.43% in the net power. As STIT is increased, the steam generation rate in the boiler reduces from 10.79 kg/s at 500°C to 10.01 kg/s at 600°C, however the enthalpy values of steam at the ST side increases causing an increase in area of the temperature entropy diagram, hence more power is obtained from the ST plant at higher ST inlet temperature. It is seen that the SOFC stack temperature also increases slightly with increase in STIT; hence the SOFC produces slightly more power at higher STIT. With STIT, the temperature of steam extracted for the PR for fuel pre-reforming increases, hence the PR exit temperature and consequently the SOFC stack temperature increases resulting in an increase of the cell voltage and SOFC power. TIT also increases slightly with STIT; however the GT power does not increase much with STIT. Since net power of the plant increases, therefore the energy and exergy efficiencies are slightly more at higher STIT. As obviously, the irreversibility in the HRSG decreases significantly with STIT due to decrease in the pinch point temperature difference at HRSG inlet. Irreversibility in the ST, condenser, BFP reduces, may be due to decrease in mass of steam produced in the HRSG. Fuel enters the PR at a fixed temperature (fixed CPR), however since the extracted steam from the ST enters the PR at higher temperature, therefore the PR exit fuel stream temperature also increases. This finally reduces the temperature difference between the state points 7 and $2'$ and consequently the PR irreversibility reduces. Irreversibility in the other system components and the exhaust irreversibility however remain invariant with STIT.

Table 3.10: Effect of ST inlet temperature on simulation results

STIT (°C)	500	525	550	575	600
SOFC power (MW)	27.75	27.87	27.87	27.99	28.10
Net GT power (MW)	23.90	23.89	23.89	23.94	23.93
Net ST power (MW)	5.67	5.79	5.89	6.00	6.11
Total power (MW)	57.32	57.55	57.65	57.93	58.14
Stack temperature (K)	980	981	981	982	983
TIT (K)	1750.5	1751.2	1751.2	1752.0	1752.7
Single cell voltage (V)	0.575	0.577	0.577	0.579	0.582
Energy efficiency (%)	55.70	55.92	56.02	56.29	56.49
Exergy efficiency (%)	54.09	54.30	54.40	54.67	54.87
Irreversibility (MW)					
HRSG	5.178	5.016	4.843	4.671	4.508
ST	1.126	1.119	1.115	1.106	1.105
COND	0.267	0.262	0.257	0.253	0.248
BFP	0.631	0.613	0.594	0.577	0.560
PR	4.077	4.064	4.052	4.039	4.026
SOFC	19.357	19.327	19.433	19.381	19.366
Combustor	10.435	10.432	10.432	10.429	10.425
GT	1.043	1.043	1.043	1.043	1.043
FR	0.509	0.509	0.509	0.509	0.509
AR	0.038	0.037	0.037	0.037	0.036
FC	0.091	0.091	0.091	0.091	0.091
AC	1.016	1.016	1.016	1.016	1.016
Exhaust	0.752	0.752	0.752	0.752	0.752
Total Irreversibility	44.520	44.281	44.174	43.904	43.685

3.7.7 Performance comparison between systems with FRAOAR and ARAOFR

In the present work, we also compared the first and second law performance of the SOFC integrated GT–ST combined cycle from two aspects. The results that we have presented above corresponds to the plant where the heat of the GT exhaust gases is first utilized for fuel preheating in the FR and then for air preheating in the AR before

utilizing it for steam generation in the HRSG. There are many proposed hybrid plants where the AR is placed ahead of the FR. But it is not known which scheme provides the better performance and there is no study on comparative performance evaluation of such a combined SOFC–GT–ST system from this aspect. The results of comparison between the two schemes are shown in Table 3.11. From the results it is seen that the proposed configuration with FRAOAR performs slightly better than the system with ARAOFR in the entire range of CPR considered. The SOFC power, net GT and ST power, both energy and exergy efficiencies are higher for the configuration with FRAOAR. Comparison of irreversibility in the system components and the total system irreversibility is shown in Table 3.12 where it is seen that not only the net power and efficiency that are more but the total system irreversibility is also less for the system with FRAOAR. Irreversibility in the two compressors (AC and FC) is not affected by the change in position of the recuperators (FR and AR) because the compressors are placed upstream of the recuperators. GT irreversibility also shows almost same values although there is difference in TIT values of the two configurations; the values are higher for the configuration with FRAOAR. Irreversibility in the HRSG, ST, condenser and BFPs of the bottoming cycle; PR and FR of the topping cycle are however less for the configuration with ARAOFR at all CPR. Irreversibility in the AR is also less for this configuration at all CPR except at CPR 6. The irreversibility in the SOFC and combustor are however less. Loss of exergy with exhaust gases is the same in both the configurations at all CPR. It is mainly the SOFC and combustor irreversibility that was responsible for slightly higher irreversibility in the configuration with ARAOFR, although the differences in total irreversibility values at a particular CPR are not that very significant.

Table 3.11: Comparison of system performance at various CPR for the configurations with FRAOAR and ARAOFR at 40 bar boiler pressure with 50% additional fuel burning

Parameter	FRAOAR					ARAOFR				
	CPR					CPR				
	6	8	10	12	14	6	8	10	12	14
SOFC power (MW)	25.65	26.73	27.34	27.78	28.10	24.37	25.63	26.50	27.06	27.51
Net GT power (MW)	18.09	20.46	22.01	23.16	23.93	17.97	20.34	21.88	23.03	23.87
Net ST power (MW)	7.38	6.88	6.53	6.29	6.11	7.30	6.80	6.47	6.22	6.03
Total power (MW)	51.12	54.07	55.86	57.22	58.14	49.64	52.77	54.85	56.31	57.41
Stack temperature (K)	982	983	983	983	983	972	974	976	977	978
TIT (K)	1743.5	1746.4	1748.5	1750.5	1752.7	1735.1	1739.1	1742.9	1746.0	1749.1
Single cell voltage (V)	0.528	0.551	0.564	0.574	0.582	0.502	0.528	0.547	0.560	0.570
Energy efficiency (%)	49.72	52.57	54.32	55.61	56.49	48.26	51.29	53.30	54.70	55.77
Exergy efficiency (%)	48.39	51.12	52.79	54.02	54.87	46.97	49.88	51.80	53.15	54.16

Table 3.12: Comparison of component and total system irreversibility at various CPR for the configurations with FRAOAR and ARAOFR

Irreversibility (MW)	FRAOAR					ARAOFR				
	CPR					CPR				
	6	8	10	12	14	6	8	10	12	14
HRSG	4.861	4.636	4.533	4.493	4.508	4.769	4.545	4.452	4.411	4.415
ST	1.048	1.049	1.063	1.078	1.105	1.036	1.036	1.050	1.064	1.089
COND	0.259	0.251	0.248	0.247	0.248	0.255	0.247	0.244	0.243	0.244
BFP	0.593	0.573	0.563	0.559	0.560	0.585	0.564	0.555	0.551	0.552
PR	4.163	4.105	4.069	4.042	4.026	4.009	3.995	3.987	3.982	3.971
SOFC	25.645	23.121	21.515	20.296	19.366	27.070	24.413	22.560	21.238	20.188
Combustor	10.587	10.531	10.489	10.455	10.425	10.617	10.558	10.511	10.474	10.442
GT	0.679	0.803	0.899	0.977	1.043	0.679	0.803	0.899	0.977	1.043
FR	0.481	0.505	0.513	0.514	0.509	0.479	0.461	0.447	0.437	0.428
AR	0.680	0.400	0.226	0.112	0.036	0.682	0.396	0.217	0.097	0.016
FC	0.062	0.072	0.080	0.086	0.091	0.062	0.072	0.080	0.086	0.091
AC	0.690	0.800	0.886	0.957	1.016	0.690	0.800	0.886	0.957	1.016
Exhaust	0.7508	0.7509	0.7511	0.7514	0.7517	0.7507	0.7509	0.7511	0.7514	0.7517
Total	50.498	47.597	45.835	44.567	43.685	51.684	48.641	46.639	45.268	44.247

3.8 Summary

A SOFC integrated combined GT–ST based power system has been simulated with the help of a mathematical model. Theoretical analysis for the hybrid system has been carried out on the basis of both the first and second law of thermodynamics. A parametric study based on variation of CPR, FFR, AFR, current density, boiler pressure, STIT and particularly the burning of additional fuel in the combustor is carried out to identify the importance of these operating parameters on energetic and exergetic performance (power, efficiency and system irreversibility) of the hybrid SOFC combined GT–ST system. Usually in a SOFC integrated combined GT–ST power cycle, the power produced by the GT and particularly the ST plant is quite less to make their integration economically feasible. Moreover small sized micro GT and particularly the ST are not very efficient at lower sizes. Therefore as a possible means of increasing the GT and ST power, the effect of additional fuel burning was studied at various CPR and it was found that bypassing some amount of fuel the SOFC and burning it in the combustor causes significant increase in the GT and ST power. However the efficiency of the plant also reduces simultaneously. While varying the CPR from 6 to 14 it was found that the efficiency of the hybrid SOFC–GT–ST plant increases with CPR for both the cases of with and without additional fuel burning. The SOFC and GT plant produces more power at higher CPR while the ST power reduces with increase in CPR. Considering the case of additional 50% fuel burning it was found that the gain in total power increases from 19.73% at CPR 6 to 27.54% at CPR 14 with corresponding decrease in efficiency of 20.91% and 15.77% at CPR 6 and 14 respectively. Further we found that the gain in total power increases with CPR while the loss of efficiency decreases. Therefore, such a combined plant with additional fuel burning needs to be operated at higher pressure for power gain from the bottoming GT and ST plant to avoid higher loss of efficiency. Moreover at CPR 14, we noticed a gain of 91.78% and 126.87% in GT and ST power respectively with 50% additional fuel burning.

From parametric variation of single level boiler pressure in the bottoming ST plant, the optimized boiler pressure was found to be 40 bar for the case with 50% additional fuel burning. At this pressure, the ST plant and the SOFC integrated combined plant produces the maximum power at a given CPR. HRSG irreversibility reduces, irreversibility in the topping SOFC–GT cycle components and the exhaust exergy loss does not change much

but the irreversibility in the other bottoming ST cycle components increases with boiler pressure, hence the total system irreversibility is more at higher boiler pressure.

Increase in FFR directly affect the net power production and efficiency of the power plant which increases linearly with FFR, however at the same time it also leads to increase in irreversible losses in the plant components including the exhaust irreversibility. Increased AFR and current density has negative effect on overall system performance, although a larger amount of air some time assists in SOFC stack cooling. Current density directly affects the SOFC stack temperature which increases with increasing current density. The SOFC and the ST plant produces more power at higher STIT, hence the plant's overall power and efficiency increases with STIT. Also the total system irreversibility is less at higher STIT; however the maximum STIT is limited by the ST blade materials.

Again the comparison of performance between the two SOFC–GT–ST configurations with FRAOAR and ARAOFR shows better performance for the presented configuration with FRAOAR. From the exergy analysis it was found that the exergy efficiency of the combined plant was less compared to the energy efficiency. The SOFC and combustor of the topping SOFC–GT cycle, the HRSG and the ST of the bottoming ST plant are the major contributors of irreversibility to the overall system irreversibility. However, when CPR is increased, the loss of exergy in these components decrease significantly, which essentially implies the importance of operating a hybrid SOFC–GT–ST plant always at higher pressure to obtain maximum benefit out of the plant. This is also evident from higher energy and exergy efficiencies obtained at higher pressure. Based on the combined energy and exergy analysis, it can be concluded that the proposed hybrid SOFC–GT–ST plant would work efficiently if it is operated at higher pressure with minimum irreversible losses in the overall system. Further some amount of additional fuel burning in the combustor bypassing the SOFC may be considered in order to boost the power output from the GT and ST plant for effective downstream integration of these two plants without much loss of efficiency and also fulfilling the thermo-economic criteria of integration.

Bibliography

[1] Chase, D.L. Combined-Cycle Development Evolution and Future. Technical Report GER-4206; (10/00), GE Power Systems, Atlanta, Georgia, United States.

[2] Gogol, T.K. A combined cycle plant with air and fuel recuperator for captive power application, Part 1: Performance analysis and comparison with non-recuperated and gas turbine cycle with only air recuperator. *Energy Conversion and Management*, 79: 771–777, 2014.

[3] Poullikkas, A. An overview of current and future sustainable gas turbine technologies. *Renew Sustain Energy Rev*, 9:409–43, 2005.

[4] Woudstra, N., Woudstra, T., Pirone A., and van der Stelt, T. Thermodynamic evaluation of combined cycle plants. *Energy Conversion Management*, 51(5): 1099-1110, 2010.

[5] Franco, A. and Casarosa, C. On some perspectives for increasing the efficiency of combined cycle power plants. Applied Thermal Engineering, 22:1501–1518, 2002.

[6] Rice, I. G. Combined cycle; The evolution of the combined cycle power plant- I. *International Turbo machinery: The global journal of energy equipment*, March 8, 2017.

[7] Haseli, Y., Dincer, I., and Naterer, G.F. Thermodynamic modeling of a gas turbine cycle combined with a solid oxide fuel cell. *International Journal of hydrogen energy*, 33:5811-5822, 2008.

[8] Park, S.K. and Kim, T.S. Comparison between pressurized design and ambient pressure design of hybrid solid oxide fuel cell–gas turbine systems. *Journal of Power Sources*, 163:490–499, 2006.

[9] Calise, F., Palombo, A., and Vanoli, L. Design and partial load exergy analysis of hybrid SOFC–GT power plant, *Journal of Power Sources*, 158:225–244, 2006.

[10] Chan, S.H., Ho, H.K., and Tian, Y. Modelling a simple hybrid SOFC and gas turbine plant. *Journal of power sources*, 109:111-120, 2002.

[11] Bavarsad, P. G. Energy and exergy analysis of internal reforming solid oxide fuel cell–gas turbine hybrid system. *International Journal of Hydrogen Energy*, 32: 4591 – 4599, 2007.

[12] Gorla, R.S.R., Pai, S.S., and Rusick, J.J. Probabilistic analysis of solid oxide fuel cell based hybrid gas turbine system. Technical Report No. NASA/TM—2003-211995, E-13666, NAS 1.15:211995, GT–2003–38046, NASA Glenn Research Center, Cleveland, OH, United States, 2003.

[13] Chan, S.H., Khor, K.A., and Xia, Z.T. A complete polarization model of a solid oxide fuel cell and its sensitivity to the change of cell component thickness. *Journal of Power Sources, 93:130*–140, 2001.

[14] Gogoi, T.K., and Das, R. Inverse analysis of an internal reforming solid oxide fuel cell system using simplex search method. *Applied Mathematical Modelling*, 37:6994–7015, 2013

[15] Massardo, A. F. and Lubelli, F. Internal Reforming Solid Oxide Fuel Cell–Gas Turbine Combined Cycles (IRSOFC–GT): Part A—Cell Model and Cycle Thermodynamic Analysis. *Journal of Engineering for Gas Turbines and Power*, 122: 27-35, 2000.

[16] Chan, S.H., Low, C.F., and Ding, O.L. Energy and exergy analysis of simple solid oxide fuel cell systems. *Journal of power sources*, 103:188-200, 2002.

[17] *JANAF Thermochemical Tables*. NSRDS-NB537, U.S. National Bureau of Standards, 2nd edition, 1971.

[18] Arsalis, A. Thermoeconomic Modeling and Parametric Study of Hybrid Solid Oxide Fuel Cell – Gas Turbine – Steam Turbine Power Plants Ranging from 1.5 MWe to 10 MWe. *Journal of power sources*, 181: 313-326, 2008.

[19] Costamagna, P., Magistri, L. and Massardo, A.F. Design and part-load performance of a hybrid system based on a solid oxide fuel cell reactor and a micro gas turbine. *Journal Power Sources*, 96: 352–368, 2001.

[20] Cengel, Y. A. and Boles, M.A. *Thermodynamics: An Engineering Approach*. Tata McGraw-Hill, 5th edition, 2006.